Sting corrections to zero-lift drag of axisymmetric bodies in transonic flow

P. R. VISWANATH and G. RAJENDRA
Experimental Aerodynamics Division
National Aeronautical Laboratory, Bangalore, India

ABSTRACT

Experiments at transonic speeds have been performed on several boat-tailed afterbodies and sting combinations with a view to assessing sting corrections to the measured afterbody drag at transonic speeds. Measurements made included afterbody total drag and base pressure in the Mach number range of 0·6-1·0 and Reynolds number range of 8-9·5 × 10^6. Correlations of base pressure and boat-tail pressure drag for the sting diameter and flare effects have been proposed using dimensional arguments. The correlations provide quick and reliable estimates for corrections that can be applied to the measured zero-lift drag of axisymmetric bodies with either contoured or conical boat-tailing.

NOMENCLATURE

A	forebody (max) cross sectional area
C_{DA}	total afterbody drag coefficient, total drag force/$(q_\infty A)$
C_{DB}	base drag coefficient, base drag/$(q_\infty A)$
C_{DF}	boat–tail skin friction drag coefficient
$C_{D\beta}$	boat–tail pressure drag coefficient, pressure drag/$(q_\infty A)$
C_f	skin friction coefficient
$C_{D\beta}{}^*$	boat–tail profile drag coefficient $(= C_{DA} - C_{DB})$
C_{pb}	base pressure coefficient
d_b	base diameter
d_m	forebody (max) diameter
d_s	sting diameter
ℓ	sting length (*see* Fig. 1)
M_∞	free stream Mach number
q_∞	free stream dynamic pressure
Re_∞	free stream Reynolds number
r	forebody (max) radius
β	boat–tail angle (*see* Fig. 1)
δ	boundary layer thickness
θ	sting flare angle

Manuscript received 22 January 1990, revised version received 17 August 1990, accepted 10 September 1990.
Paper No 1769.

1. INTRODUCTION

Wind tunnel testing of aircraft, missile and other axisymmetric models generally involves rear-mounted sting supports and the aerodynamic interference offered by them continues to be a problem, particularly at transonic Mach numbers. The aerodynamic quantity most affected is the drag of the afterbody in view of its proximity to the support system, although effects on lift and pitching moment can be important in many cases. Reliable methods for providing corrections to the measured data are required before the data can be used in design or for extrapolation to flight conditions. The flow field behind a blunt base in the presence of the support system is sufficiently complex that rational prediction procedures for determining corrections would involve elaborate computing and hence are not generally suitable for day-to-day wind tunnel testing practice. The emphasis in literature therefore has been to suggest empirical correlations for sting effects (*see* Cahn[1], McDonald and Hughes[2]).

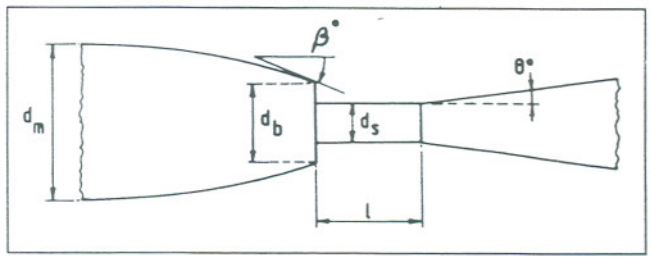

Figure 1. Sketch defining afterbody and sting geometrical parameters.

The total afterbody drag coefficient, C_{DA}, which is composed of the boat–tail pressure drag, $C_{D\beta}$, the boat–tail skin friction drag, C_{DF}, and the base drag, C_{DB}, depends on a number of geometrical parameters of the afterbody and sting and relevant flow parameters ahead of the afterbody. A schematic of an afterbody–sting combination, defining various geometrical parameters is shown in Fig. 1. Sting effects may be classified under sting diameter and flare effects, the latter depending on the location of flare from the base. For $\ell \to 0$ or $d_b/\ell \to \infty$, the flare begins at the model base and we shall refer to this geometry as *a tapered sting*.

As ℓ increases, the flare effect will decrease and the sting diameter effect dominate. For $\ell \to \infty$ or $d_b/\ell \to 0$, only the sting diameter effect will be present.

Experimental investigations have provided the most valuable information on sting effects. Although a large body of data on sting effects exist in literature (*see* Tuttle and Gloss[3]; Tuttle and Lawing[4]), systematic studies at transonic speeds devoted to providing data even for correlation purposes are very few. A major source of data resulted from a systematic parametric study carried out by Cahn[1] in the Mach number range of 0·8 to 1·10 and Reynolds number range of 15-17·4 $\times$ 10^6. Based on tests on a variety of afterbody–sting combinations, he presented an approximate (empirical) method for sting corrections, valid in the limited Mach number range (and Reynolds number) of the tests, and for the different afterbody geometries studied. However, the experiments made by Cahn included very few afterbody models with $\beta<16°$, which are more often encountered in practice. McDonald and Hughes[2] utilised Cahn's as well as other data including jet effects and presented a method of correlation of afterbody drag in the presence of a propulsive jet or a support sting. Their empirical correlations, derived from a careful analysis of data (on both contoured and conically boat-tailed bodies) at a Mach number of 0·9, were assumed valid in the Mach number range 0·6 to 0·9 and for attached flow on the afterbody. The general validity or the usefulness of their correlation (based on limited data available at that time) does not seem to have been assessed in the literature. Sykes[5] suggested a correlation for the total afterbody drag based on a limited series of tests on two conically boat-tailed afterbodies (with β = 7·5° and 9°) in the Mach number range 0·7 to 1·15. In addition, he modified an expression given by Tunnell[6] for the flare effect and proposed a correlation for the base pressure which is applicable for $\ell/d_b \geq 2$ and shows that the flare effect diminishes for $\ell/d_b \geq 6$.

From the preceding discussion it appears evident that not much useful data exists in the literature even for attempting generalised correlations for sting effects on the afterbody drag at transonic speeds. Most earlier studies have dealt with specific afterbody–sting combinations, possibly because of their relevance in practical applications. The present work is an attempt to fill this lacuna to some degree and to provide generalised correlations useful for quick estimation of sting corrections. Tapered stings ($\ell \to 0$) are investigated in detail in this work in view of their wide application; correlations for sting diameter effect are also included.

2. EXPERIMENTS

Experiments have been performed in a 38 cm $\times$ 30 cm transonic wind tunnel in the Mach number range 0·7 to 1·0. The free stream Reynolds number based on model length of 30·5 cm (*see* Fig. 2) varied between 8 $\times$ 10^6-9·5 $\times$ 10^6 in the above Mach number range.

2.1 Model support system

A sketch of the model support system along with the afterbody model and sting is shown in Fig. 2. The instrumented part consists of a 30 mm long cylindrical section and a removable afterbody 100 mm long (Fig. 2). The balance (designed for an axial load of 2·25 kg) measures the total axial force experienced by the instrumented part of the model and provides direct measurement of total drag changes due to the presence of the sting. Base pressure is measured at a single location on the model centreline. The stings were fixed from the rear portion of the fork support system so that there was a narrow gap (about 0·5 mm) between the base plane and the front face of the sting. This arrangement enabled the quick removal and fixing of different stings.

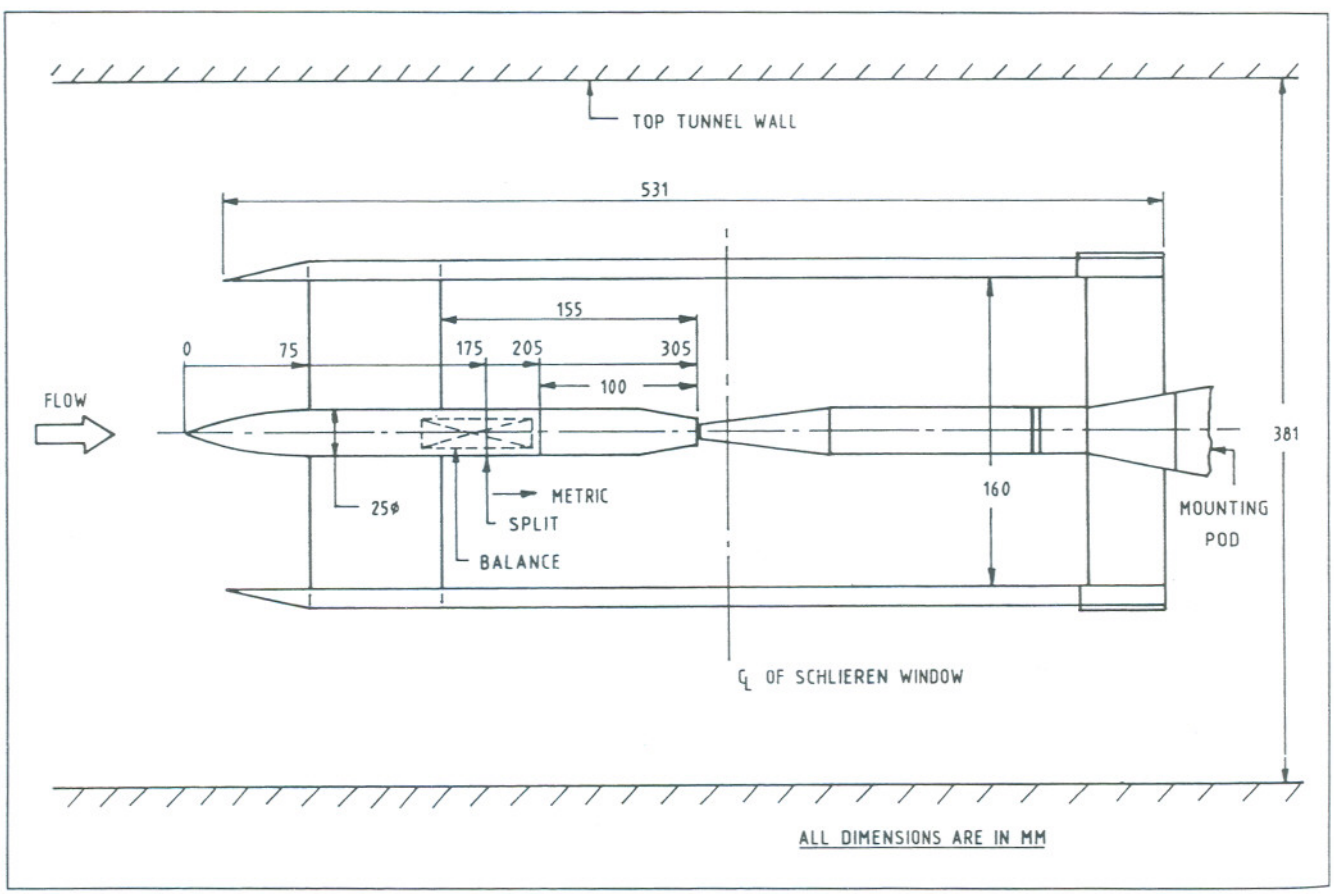

Figure 2. Sketch of model-sting support system.

All tests were carried out at zero incidence. The model boundary layer was tripped (using carborundum grit of size 40 over a width of 12 mm) in the nose region at a distance of 25 mm from the apex. In view of the relatively high unit Reynolds number of the free stream (about $0{\cdot}3 \times 10^6$ per cm), we expect transition to have occurred immediately downstream of the trip with a turbulent boundary layer growing over a large part of the model. The measured sting-free base pressure levels, for example, on different boat-tailed afterbodies (as well as on a cylindrical afterbody[7]) strongly support the above view; the data indicate (figure not shown) broad agreement with what would be expected with turbulent boundary layer flow on the afterbody (*see* Cahn[1], Cubbage[8]).

2.2 Afterbody models and stings

Table 1 shows the geometric details of the various afterbody models tested. Two circular arc and four conically boat-tailed models were chosen for this study with a view to complement the data set of Cahn; the boat-tail angles were selected to be in the lower range ($\beta \leq 16°$) to be useful in practical applications.

The geometric details of various tapered stings (S1-S6) tested are shown in Fig. 3; the taper or flare angle was varied in the range 1·5° to 5° again to complement the data of Cahn. To assess the sting diameter effects, tests were also made on four cylindrical stings having diameters of 6·25, 8·35, 11·8 and 16 mm.

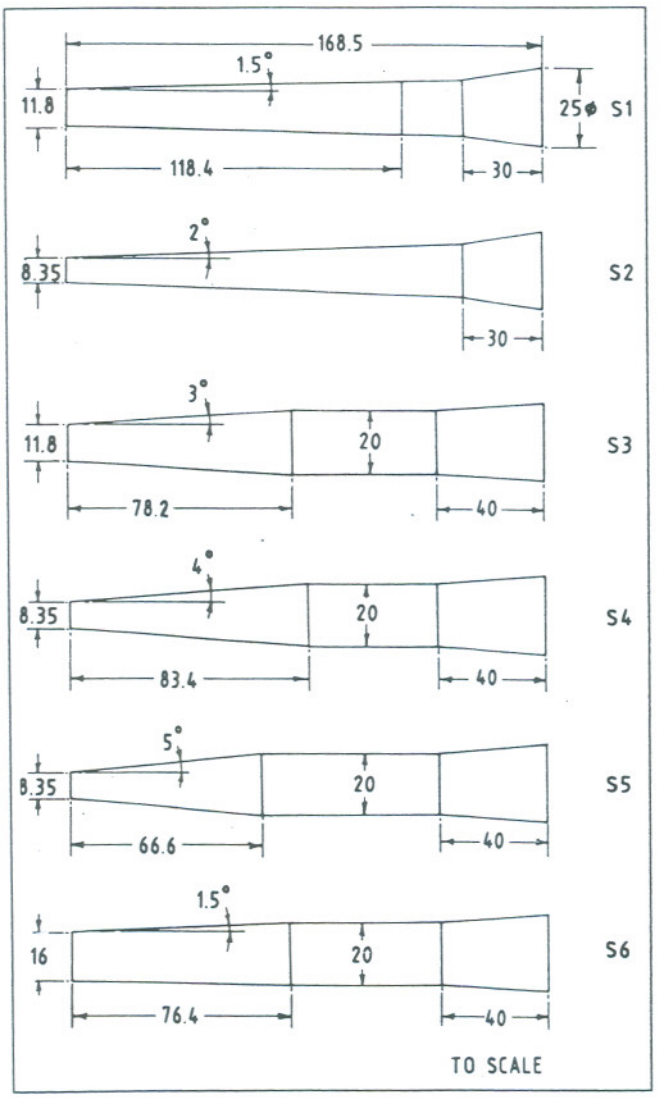

Figure 3. Sketch of tapered stings.

TABLE 1
Geometric details of afterbody models

Geometry	Notation	d_m, mm	d_b, mm	β, deg
CIRCULAR ARC	CA–5	25	18·2	5*
	CA–12	25	12·6	12*
CONICAL	CO– 4	25	16	4
	CO– 8	25	12·8	8
	CO–12	25	12·8	12
	CO–16	25	13·0	16

* Angle at the base plane
Length of afterbody models: 100mm

2.3 Measurements

Axial force of the afterbody was measured with a balance described earlier. The uncertainty in these measurements was within ±0·009 kg. The base pressure and the pressure in the gap between the two body sections (at the split) were both measured relative to the free stream static pressure using differential transducers each having a range of 35 kPa.

Assessment of flow separation ahead of the model base was made using colour Schlieren technique, and for some configurations surface oil flow visualisation was also used.

2.4 Assessment of wall and support system interference

In planning the experiments, sufficient care was taken to minimise possible interferences on the measurements either from the walls or the support system. The top and bottom tunnel walls were slotted with an open area ratio of 8% and the maximum solid blockage of the model (including the support system) was about 1·3% which is small enough for any blockage effect to be insignificant. The fork support system used has similarities with the systems used in sting interference studies (Cahn[1], Gloss and Sewall[9]). Minor interference effects from the support system, if any, should not materially affect the measured data since the primary interest in this work is to determine "changes in afterbody drag due to sting effects" rather than the (absolute) drag values. Further evidence in support of this view is contained in Section 3.3.

3. RESULTS AND DISCUSSION

Before presenting in detail the results for the sting diameter and flare effects, we first examine the likely effects of "sting positioning" employed in this study; the sting was not introduced inside the afterbody (unlike in conventional testing practice), but formed a narrow gap between the base and the front face of the sting. Measurements were made on a typical contoured afterbody (with $d_b/d_m = 0{\cdot}5$ and $\beta = 8°$) with both sting configurations mentioned above. Results of base pressure coefficient, C_{pb}, and boat–tail profile drag coefficient, $C_{D\beta}$*, (Fig. 4) shows excellent agreement between the two configurations suggesting that the scheme adopted in this study provides realistic sting effects.

In what follows, we present typical results sufficient for further analysis and discussion. A detailed account of this investigation containing all the results is available in Ref. 10.

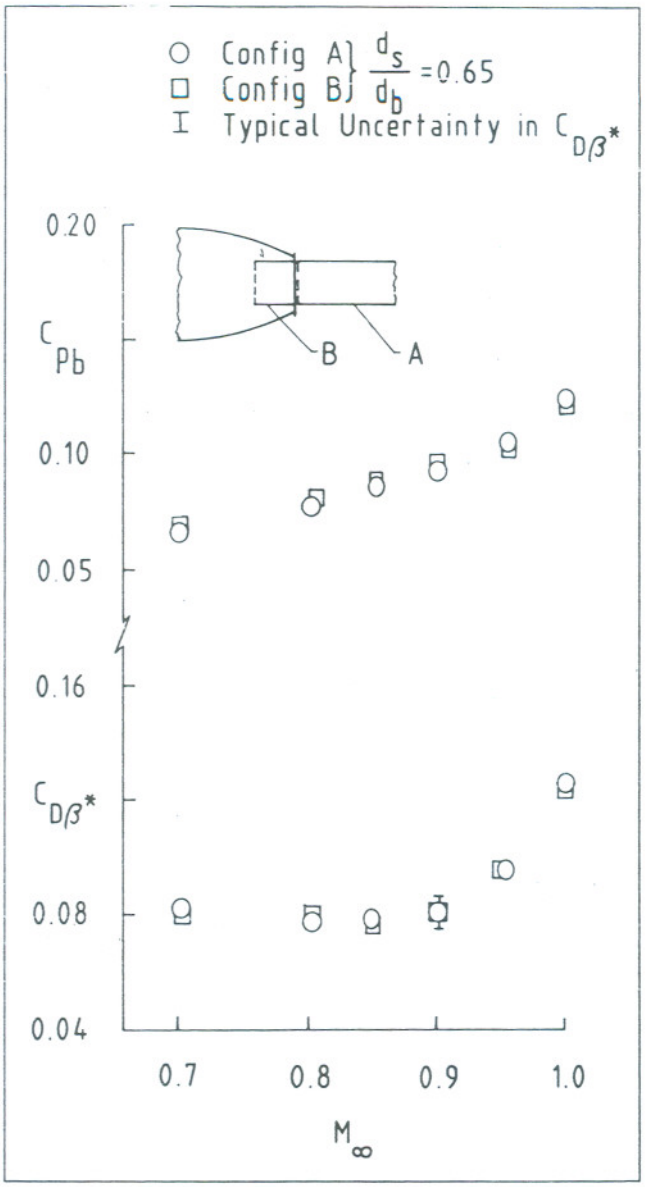

Figure 4. Effect of sting positioning on base pressure and drag.

3.1 Sting diameter effects

Typical results of base pressure coefficient C_{pb} and boat–tail profile drag coefficient $C_{D\beta}{}^*$ for three afterbodies are shown in Figs 5-7 with sting diameter as a variable. The vertical bar in these figures (and many to follow) indicates the estimated typical uncertainty in $C_{D\beta}{}^*$. Lines have been drawn through the data in these figures for visual clarity. At each Mach number, there is a progressive increase in the base pressure and a reduction in boat–tail drag with an increase in the sting diameter. These are qualitatively similar to the results obtained in many earlier studies (e.g. Sykes and Cahn). The reduction in $C_{D\beta}{}^*$ is caused by the positive pressure field (the upstream influence effect on potential flow) imposed on the afterbody due to the sting. The increase in base pressure with sting diameter is caused by the progressive decrease in the (axisymmetric) step height to boundary layer thickness at separation.

Interestingly, for each sting, the changes in base pressure and $C_{D\beta}{}^*$ relative to $d_s = 0$ appear to be nearly the same over the range of M_∞ covered except for around $M_\infty = 1$. In the neighbourhood of $M_\infty = 1{\cdot}0$, the base flow field and the drag variation are known to be complex and very sensitive to M_∞ (e.g. Swamy *et al*[11]). For all the above cases, the flow on the afterbody was attached as revealed by Schlieren visualisation.

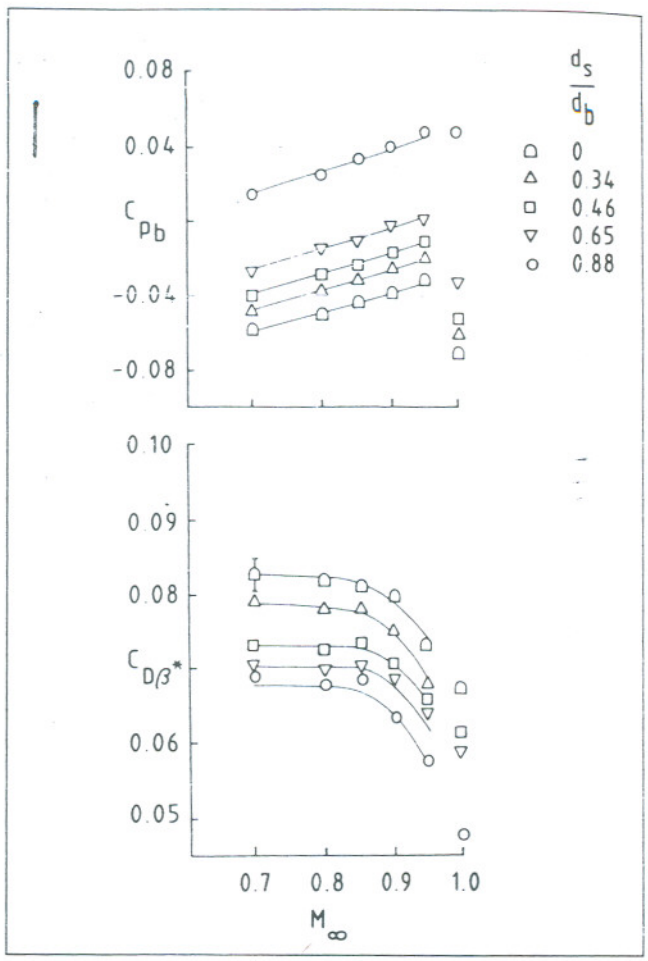

Figure 5. Sting diameter effects: Model CA-5.

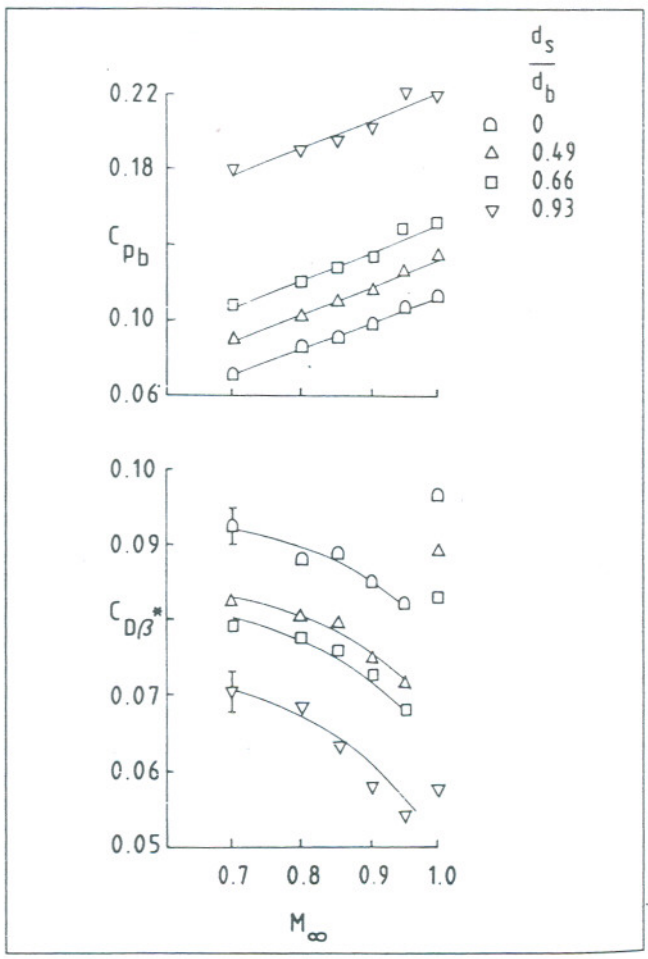

Figure 6. Sting diameter effects: Model CA-12.

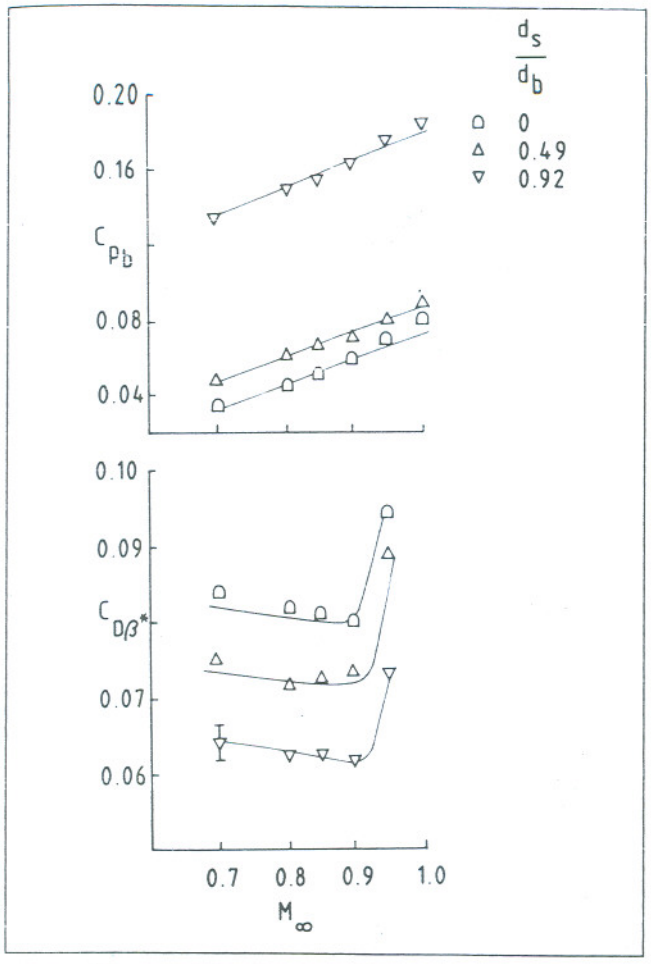

Figure 7. Sting diameter effects: Model CO-8.

The results for the afterbody CO-16 (Fig. 8) shows a different trend for C_{pb}; base pressure decreases with M_∞, and further, the changes in C_{pb} relative to the no sting case has a strong dependence on Mach number. Schlieren and surface oil flow observations showed separated flow on the afterbody for $M_\infty = 0{\cdot}90$ even in the absence of the sting; the constancy of C_{pb} at $M_\infty = 0{\cdot}95$ and $1{\cdot}0$ in the presence of the sting is a feature that can be expected due to separated flow ahead of the base. The boat–tail profile drag, on the other hand, still reflects some features qualitatively similar to the unseparated cases discussed earlier.

3.2 Sting flare effects

Flare effects were studied on all the afterbodies shown in Table 1 with the exception of CO-16, which involved afterbody flow separation even in the absence of the sting. It was apparent that the results with flow separation would exhibit a different behaviour compared to attached flow. Tests with tapered stings therefore were not made on CO-16 since the flow separation would then be aggravated further.

Figures 9 and 10 display results of C_{pb} and $C_{D\beta}{}^*$ for two afterbodies and tapered sting combinations; results for the diameter effect alone are also included in these figures to enable the assessment of flare effects for a fixed value of d_s/d_b. These results exhibit trends qualitatively similar to the sting diameter effect. As may be expected, both the base drag and boat–tail profile drag decrease further due to the presence of a flare. Interestingly, as with the sting diameter effects, the changes in C_{pb} and $C_{D\beta}{}^*$ due to the flare angle appear nearly insensitive to the free stream Mach number except around $M_\infty = 1$. The absence of flow separation for all the data shown in Figs 9 and 10 was again confirmed by Schlieren observations.

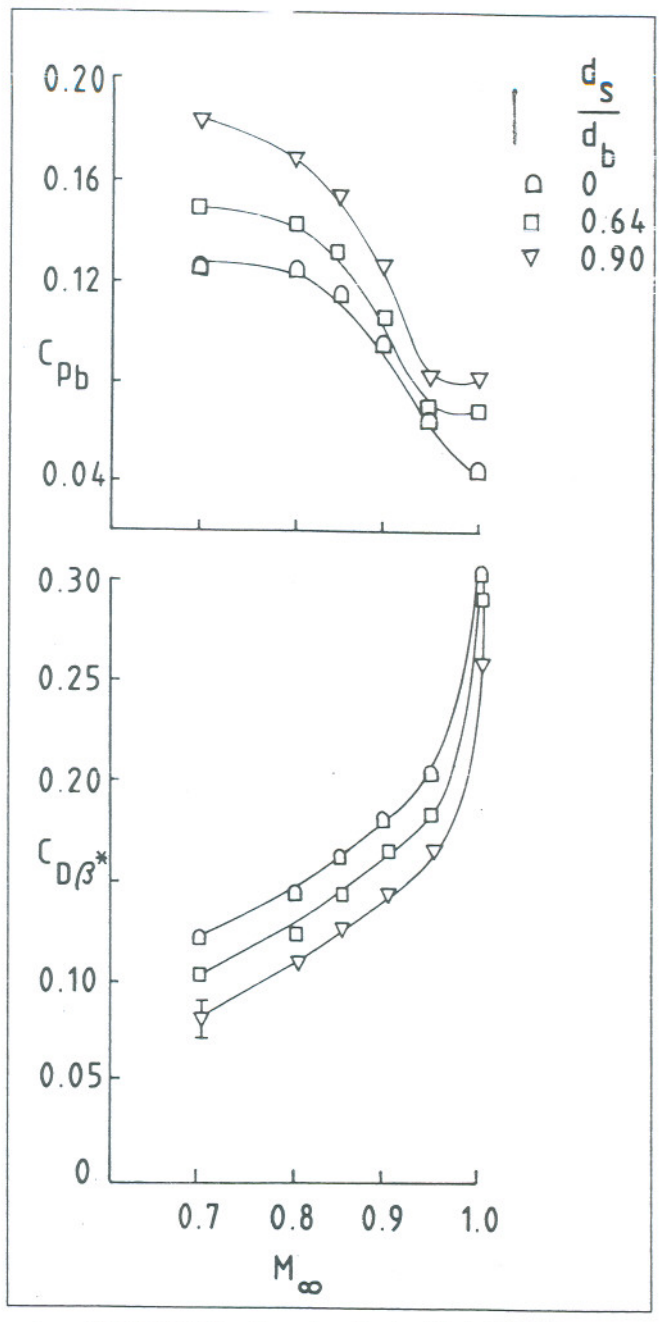

Figure 8. Sting diameter effects: Model CO-16.

3.3 Correlations

The results of base pressure and boat–tail profile drag as influenced by the geometrical parameters of the sting (Figs 5-10) suggest that correlations may be sought for the *changes* in base pressure and boat–tail pressure drag due to sting diameter and flare effects. The two effects are considered *separate* and assumed *additive*.

We may write

$$\Delta C_{pb} = \Delta C_{pb(d_s)} + \Delta C_{pb(\theta)}$$

$$\Delta C_{D\beta} = \Delta C_{D\beta(d_s)} + \Delta C_{D\beta(\theta)}$$

where ΔC_{pb} and $\Delta C_{D\beta}$ represent the total change in C_{pb} and $C_{D\beta}$, respectively, due to sting diameter and flare effects. With turbulent boundary layer flow on the afterbody at high Reynolds numbers, in general, we may expect the base pressure and the boat–tail pressure drag to depend on

M_∞, Re_∞ (flow parameters),
d_m, d_b, β (afterbody geometrical parameters), and
d_s, θ (sting geometrical parameters).

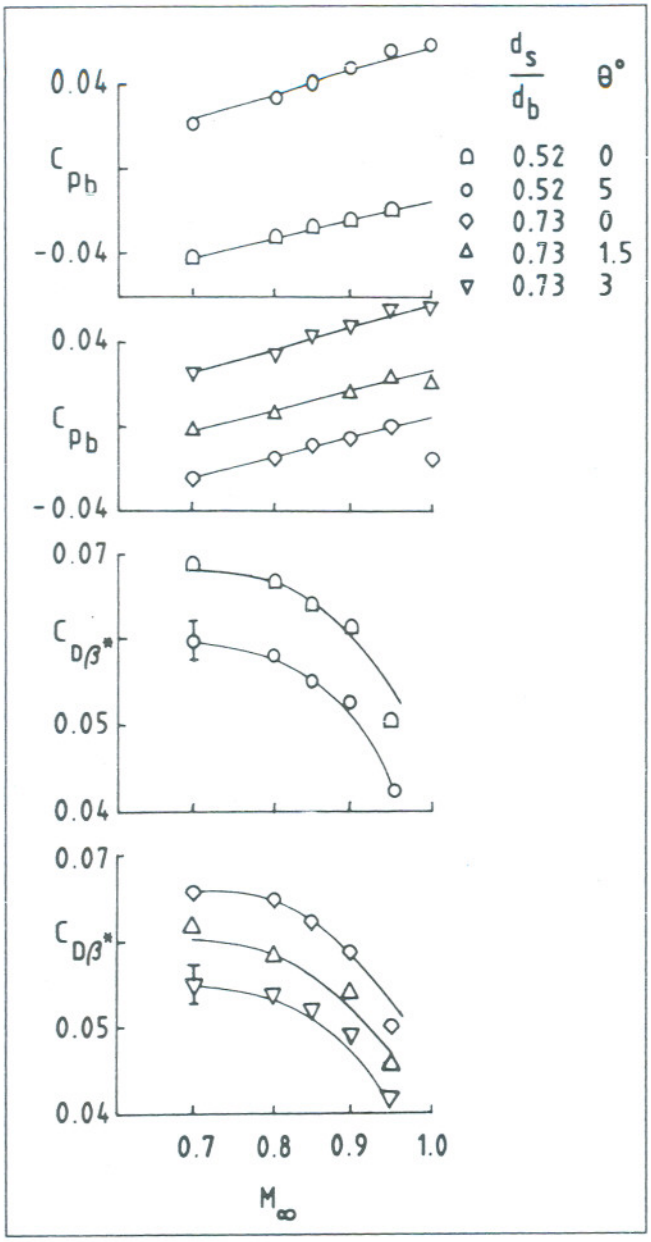

Figure 9. Sting flare effects: model CO-4.

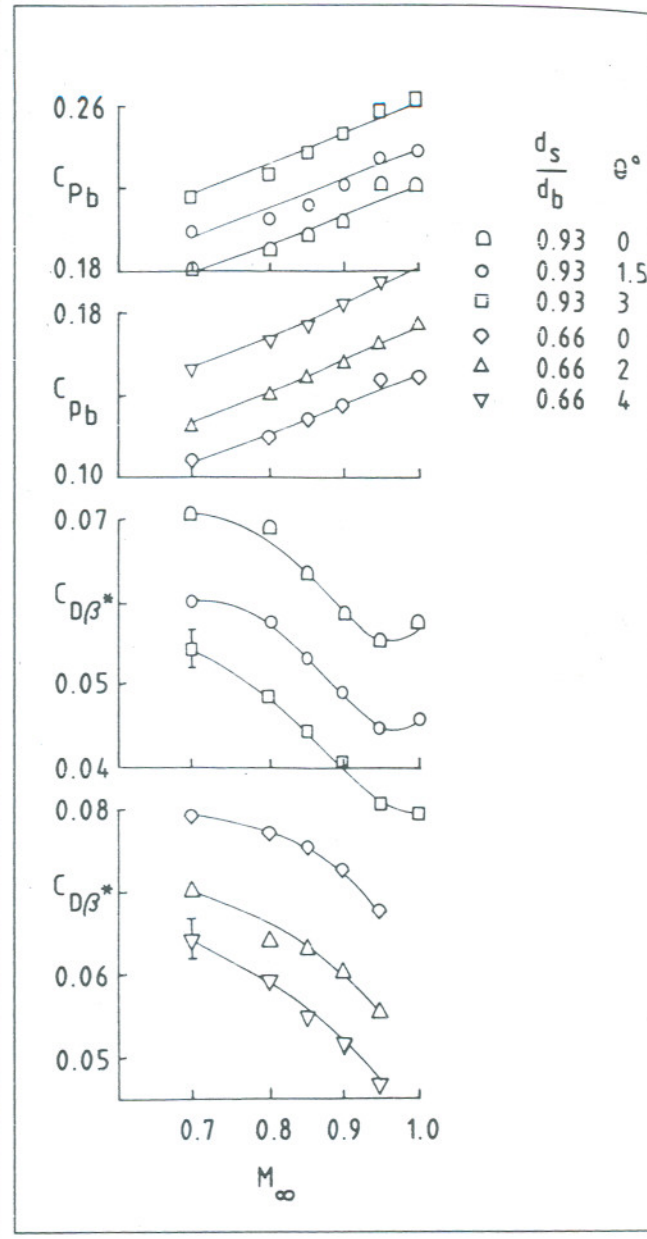

Figure 10. Sting flare effects: Model CA-12.

Using dimensional analysis, we may write *for a tapered sting*,

$$C_{pb(d_s,\theta)} = F_1(M_\infty, Re_\infty, d_b/d_m, \beta, d_s/d_b, \theta) \quad . \; . \; . \quad (1)$$

$$C_{D\beta(d_s,\theta)} = F_2(M_\infty, Re_\infty, d_b/d_m, \beta, d_s/d_m, \theta) \quad . \; . \; . \quad (2)$$

Equations (1) and (2) are now utilised to write the following expressions for the diameter and flare effects respectively:

(a) Sting diameter effect: ($\theta = 0$)

For fixed values of (M_∞, Re_∞, d_b/d_m, β), we have

$$\triangle C_{pb(d_s)} = C_{pb(d_s,0)} - C_{pb(0,0)} = f_1(d_s/d_b) \quad . \; . \; . \quad (3)$$

$$\triangle C_{D\beta(d_s)} = C_{D\beta(d_s,0)} - C_{D\beta(0,0)} = f_2(d_s/d_m) \quad . \; . \; . \quad (4)$$

(b) Sting flare effect:

For fixed values of (M_∞, Re_∞, d_b/d_m, β, d_s/d_b), we have

$$\triangle C_{pb(\theta)} = C_{pb(d_s,\theta)} - C_{pb(d_s,0)} = f_3(\theta) \quad . \; . \; . \quad (5)$$

$$\triangle C_{D\beta(\theta)} = C_{D\beta(d_s,\theta)} - C_{D\beta(d_s,0)} = f_4(\theta) \quad . \; . \; . \quad (6)$$

We now examine the usefulness of the relationships given by equations (3), (4), (5) and (6) and assess the sensitivity of other parameters by plotting the data obtained in the present experiments as well as those of Cahn.

For the present tests, the change in boat–tail pressure drag ($\triangle C_{D\beta}$) was inferred in the following manner. For each afterbody and given flow conditions, the variations in C_f (on the afterbody) with and without the sting were assumed small; these variations arise from the slightly altered pressure field on the afterbody due to the presence of the sting. This assumption was verified by comparing skin friction distributions obtained from computer codes for both inviscid and turbulent boundary layer flow (with and without a sting), for a few cases of contoured afterbodies at a Mach number of 0·8. For each afterbody–sting combination, $\triangle C_{D\beta}$ was therefore inferred by appropriate subtraction of the values of $C_{D\beta}{}^*$. For example,

$$\triangle C_{D\beta(d_s)} = C_{D\beta}{}^*{}_{(d_s,0)} - C_{D\beta}{}^*{}_{(0,0)}; \text{ and}$$

$$\triangle C_{D\beta(\theta)} = C_{D\beta}{}^*{}_{(d_s,\theta)} - C_{D\beta}{}^*{}_{(d_s,0)}.$$

The correlation plots are shown in Figs 11-14; each symbol in these figures represent a given afterbody–sting combina-

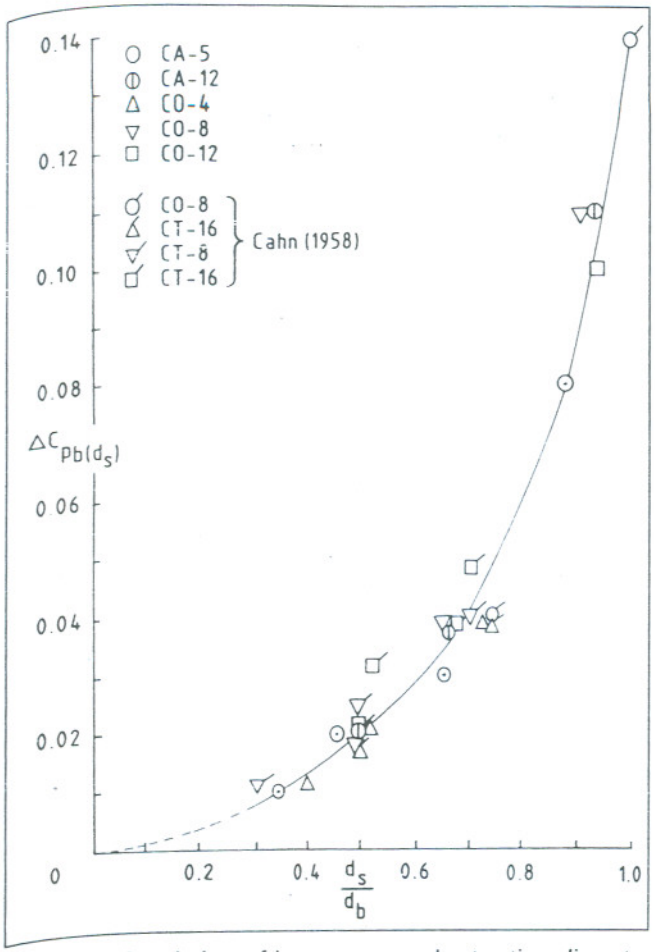

Figure 11. Correlation of base pressure due to sting diameter effect.

tion. We have further utilised the observation (discussed in Section 3.1 and 3.2) that the changes in C_{pb} and $C_{D\beta}{}^*$ are sensibly independent of Mach number in the range 0·7 to 0·95.

The data plotted in the non-dimensional parameters suggested by equations (3) and (4) for the sting diameter effect are shown in Figs 11 and 12. Excellent correlation of base pressure may be seen (Fig. 11) which suggests that $\Delta C_{pb(d_s)}$ is determined by local geometrical parameters, and sensibly independent of free stream Reynolds number as well as the afterbody shape. On the other hand, the changes in

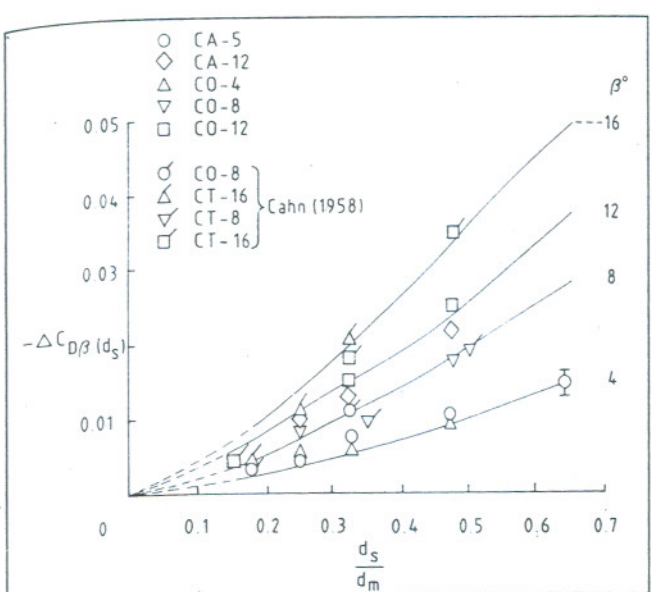

Figure 12. Correlation of boat–tail pressure drag due to sting diameter effect.

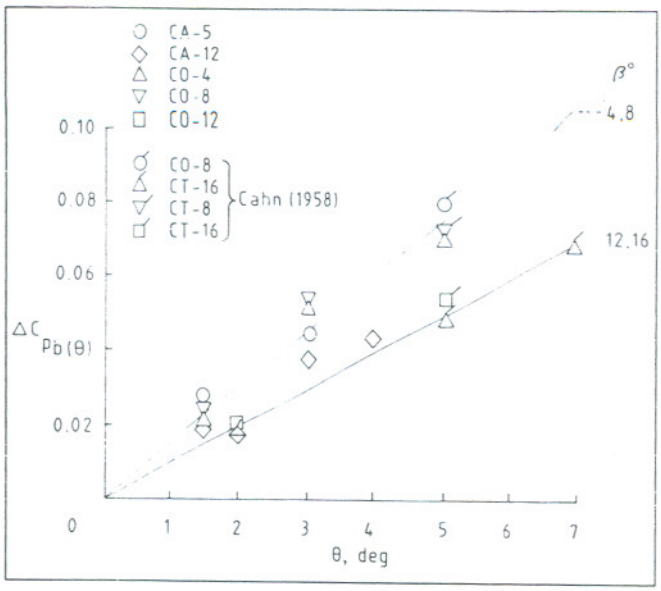

Figure 13. Correlation of base pressure due to sting flare effect.

boat–tail pressure drag (Fig. 12), show dependence on two afterbody geometrical parameters. This is understandable since at least two parameters are required to characterise the afterbody shape. Increased drag reduction with increasing β (for a fixed value of d_s/d_m) perhaps reflects the increased upstream effect of the sting at higher β.

Correlations for the sting flare effects, in the non-dimensional parameters given by equations (5) and (6), are shown in Figs 13 and 14. Except for a dependence on β, no systematic effect of other afterbody shape parameters can be discerned. The increased drag reduction with increasing β (for any given value of θ) is again to be expected (Fig. 14) based on upstream effect considerations; the lower base pressure changes seen at the higher β (Fig. 13) is likely to be an effect of the retarded boundary layers ahead of separation due to the higher adverse pressure gradients on the afterbody.

The success of the correlations (Figs 11-14) reveals *two important factors*. First, the consistency and agreement of the base pressure and drag data obtained in the two investigations; the afterbody pressure drag was obtained by integration of surface pressures in Cahn's work, as opposed to the use of balance in the present tests. Second, the insensitivity of the correlations to the free stream Reynolds number between Cahn's experiments and the present work (a factor of two).

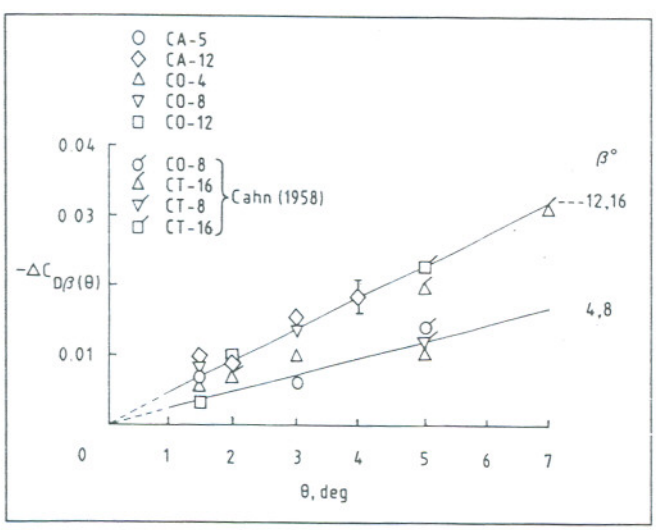

Figure 14. Correlation of boat–tail pressure drag due to sting flare effect.

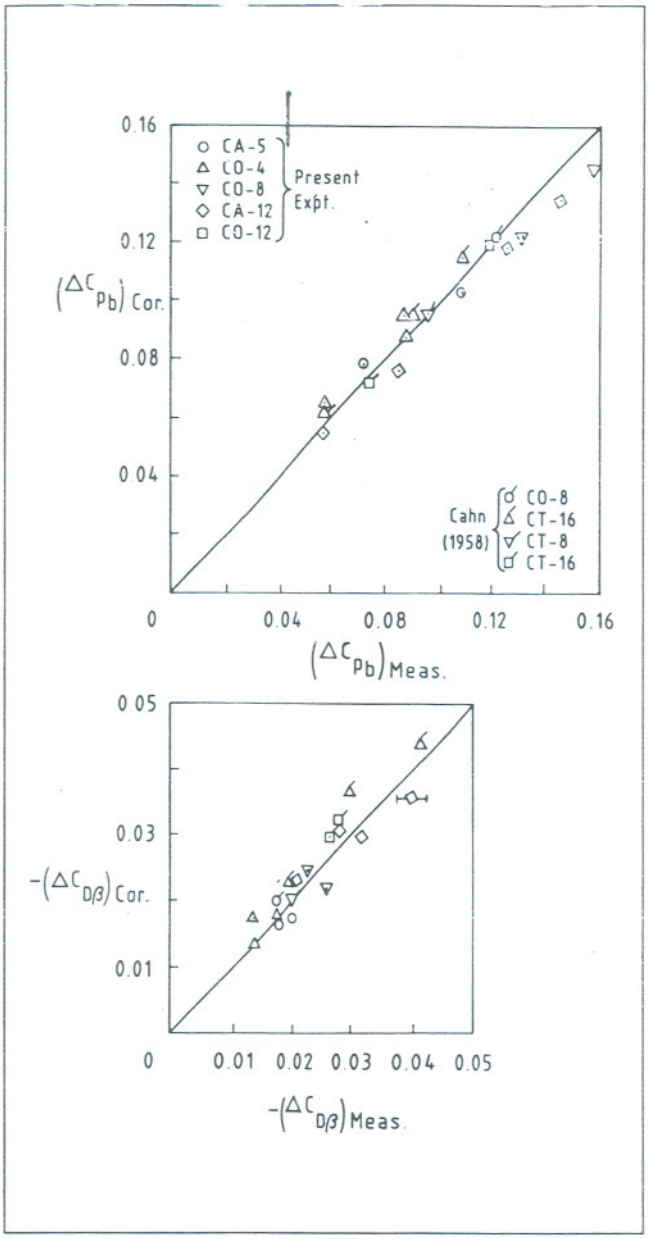

Figure 15. Comparison of measured corrections with estimates from correlations: Present data and Cahn.

To enable quick estimates of sting corrections for use in practical applications, simple expressions are fitted for the lines drawn through the data in Figs 11-14. These expressions (described in Appendix 1) are shown plotted in Fig. 15 against our measurements as well as those of Cahn which indicates very good agreement consistent with the accuracy of the measured data.

3.4 Comparison with additional test cases

With a view to assessing the validity of the above correlations further, *several new test cases* involving different afterbody–sting combinations were generated as a part of this study. These configurations are shown in Fig. 16 and measurements were made *with and without the sting* in the Mach number range 0·7-0·95. Additional test data was also obtained at a free stream Mach number of 0·6 for examining the effectiveness of the correlations at lower Mach numbers.

Figure 17 shows comparisons of the estimates using expressions A1-A4 with actual measurements of sting effects for all the test cases described above. The agreement is seen to be at least as good as in Fig. 15 (which provided data for the correlations), except possibly for the case CT-12/S9 in which a tapered sting (using the definition adopted here) is

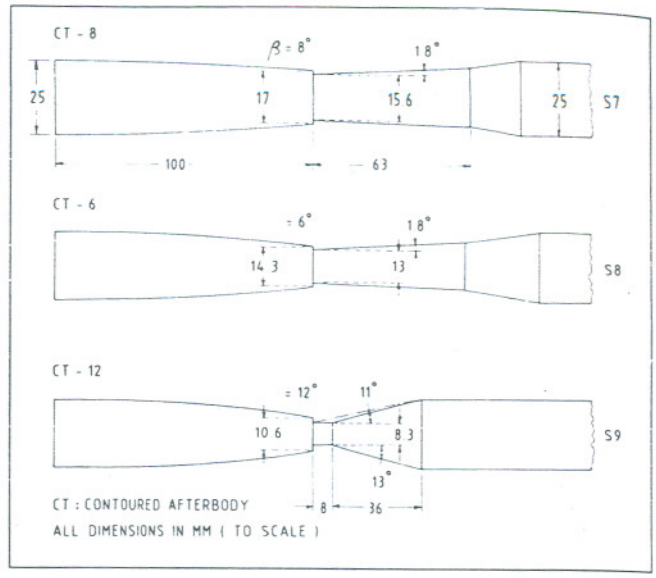

Figure 16. Sketch defining afterbody–sting combinations: New test cases.

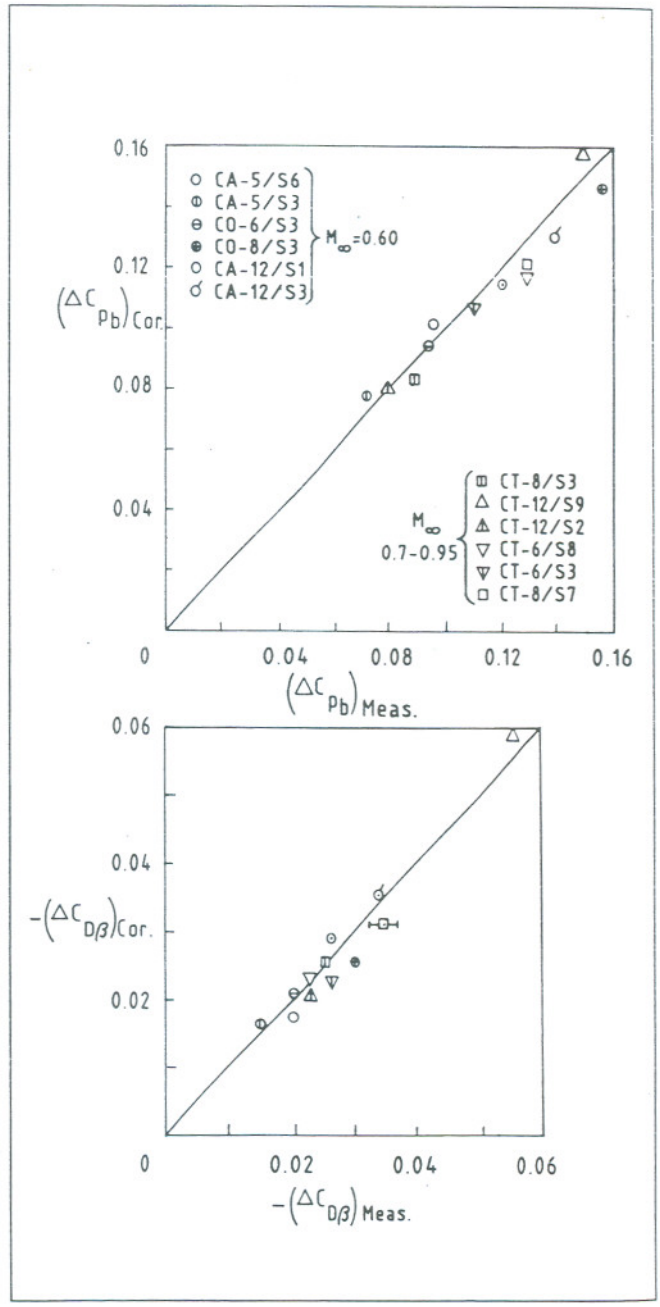

Figure 17. Comparison of measured corrections with estimates from correlations: New test cases and data at M_∞ = 0·60.

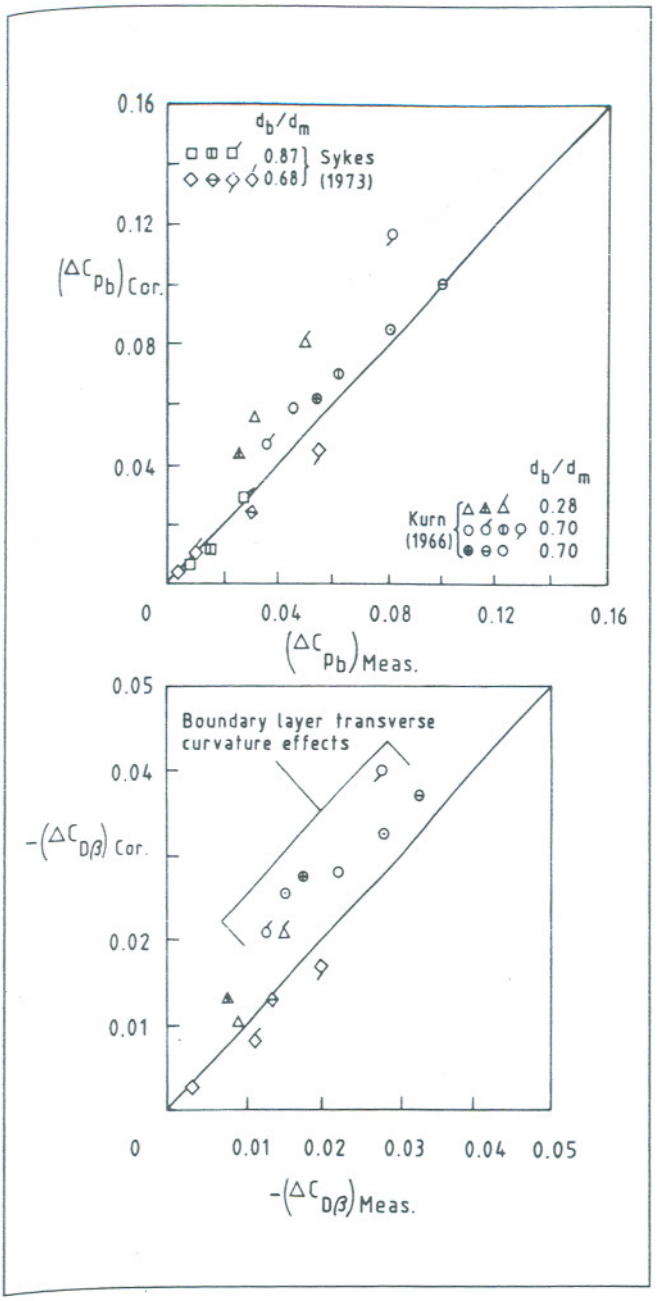

Figure 18. Comparison of measured corrections with estimates from correlations: Data of Sykes and Kurn.

not used. Estimates shown for this case have been made for the equivalent flare angle of 11° (shown by a chain line in Fig. 16) which seem to compare reasonably well with the measurements although the value of θ (= 11°) is outside the range of flare angles used to establish the correlations. The agreement of all test cases at $M_\infty = 0{\cdot}6$ may also be seen to be excellent.

3.5 Comparison with earlier data

Earlier data reported by Sykes[5] on two conical boat–tails and of Kurn[12] on two tangent ogive afterbodies are examined in the light of the present correlations. Kurn's data correspond to tapered stings while Sykes' data are on diameter effects. Comparisons with the estimates from the correlations (Fig. 18) show good agreement with Sykes' data*, while the measured sting effects are consistently lower in Kurn's experiments.

*Correlation estimates of ($\Delta C_{D\beta}$) for the afterbody with $d_b = 0{\cdot}87 d_m$ have not been included in Fig. 18 since, for reasons not clear to us, the data shows only a small change in $\Delta C_{D\beta}$ over a significant variation of d_s/d_b.

Since the model configuration used by Kurn involved a long forebody (a cylinder extending all the way into the contraction of the wind tunnel), as opposed to a finite forebody (with a fineness ratio in the range 6-7) in the present as well as Cahn's tests, it was logical to examine if the observed differences above could be due to the boundary layer transverse curvature effects in Kurn's data. Estimates of curvature parameter (δ/r) at the beginning of the afterbody shows that it is about 0·87 in Kurn's experiments but ranges between 0·18 and 0·21 in the others. This view gets added support from the observed better agreement (in a relative sense) of ΔC_{pb} (Fig. 18) with an increase in base diameter from 0·28 to 0·70 d_m in Kurn's tests, although such an improvement is not evident in the $\Delta C_{D\beta}$ comparisons. Apparently, boundary layer transverse curvature effects can affect the base pressure and boat–tail pressure drag significantly. With the available data, we suggest that the correlations should be used with some caution in cases where (δ/r) $\geq 0{\cdot}20$. It would be informative to determine (in future work) the critical value of (δ/r) upto which the correlations developed here can be applied with confidence.

4. CONCLUSIONS

An experimental investigation has been carried out primarily for providing reliable data for assessing sting corrections on afterbody drag at transonic speeds. Experiments have been made on several afterbodies and sting combinations in the Mach number range of 0·6-1·0 and Reynolds number range of 8-9·5 × 10^6. Measurements made included afterbody total drag (using a balance) and base pressure. Correlations of base pressure and boat–tail pressure drag for the sting diameter and flare effects have been proposed using dimensional arguments. The effectiveness of these correlations have been assessed by comparison with additional test cases generated in this study and with earlier data. The correlations provide quick and reliable estimates of corrections to the measured zero-lift drag of axisymmetric bodies, and are expected to be valid under the following conditions.

1. Contoured afterbodies:

$0{\cdot}6 \leq M_\infty \leq 0{\cdot}95$; $4° \leq \beta \leq 16°$
$0{\cdot}2 \leq d_s/d_b \leq 0{\cdot}95$; $\theta \leq 5°$
$0{\cdot}25 \leq d_s/d_m \leq 0{\cdot}70$

2. Conically boat–tailed afterbodies:

$0{\cdot}6 \leq M_\infty \leq 0{\cdot}90$; $4° \leq \beta^+ \leq 12°$
$0{\cdot}2 \leq d_s/d_b \leq 0{\cdot}95$; $\theta \leq 5°$
$0{\cdot}25 \leq d_s/d_m \leq 0{\cdot}70$

+ (If $\beta \leq 8°$, the correlations are valid up to $M_\infty = 0{\cdot}95$).

The most important requirement for the applicability of the correlations is that the turbulent boundary layer flow on the afterbody *must be attached under all conditions*. Otherwise, no evidence of Reynolds number effect has been observed in the correlations. Flow separation on the afterbody can give rise to effects very different from those studied here.

It is unlikely that generalised correlations of the kind proposed here can be extended to higher transonic Mach numbers (say, 1·0-1·20) since the flow field, in general, may be expected to be highly Mach number sensitive; furthermore, the data may become sensitive to the details of the afterbody shape, model support system and interference from tunnel walls.

ACKNOWLEDGEMENT

The authors express their sincere thanks to all the members of the 0·3 m Tunnel Group for their assistance and cooperation in carrying out the experiments, and the staff of the Model Shop for the model fabrication. Thanks are due to Dr S. S. Desai for providing numerical results from a transonic flow code (both inviscid and viscous) and for helpful discussions.

REFERENCES

1. CAHN, M. S. An Experimental Investigation of Sting Support Effects on Drag and a Comparison with Jet Effects at Transonic Speeds, NACA Report 1353, 1958.
2. MCDONALD, H. and HUGHES, P. F. A correlation of subsonic afterbody drag in the presence of a propulsive jet or support sting, *J Aircr*, 1965, **2**, pp 202-207.
3. TUTTLE, M. H. and GLOSS, B. B. Support Interference of Wind Tunnel Models – A Selective Annotated Bibliography, NASA TM 81909, 1981.
4. TUTTLE, M. H. and LAWING, P. L. Support Interference of Wind Tunnel Models – A Selective Annotated Bibliography, Supplement to NASA TM 81909, 1984.
5. SYKES, D. M. Sting Interference Effects on Afterbodies at Transonic Speeds, AGARD CP 124, Paper No. 27, 1973.
6. Tunnell, P. J. Investigation of Sting–Support Interference on Base Pressure and Forebody Chord Force at Mach Number from 0·6 to 1·3, NACA RM A54 K16a, 1954.
7. VISWANATH, P. R. Passive devices for axisymmetric base drag reduction at transonic speeds, *J Aircr*, 1988, **25**, (3), pp 258-262.
8. CUBBAGE, J. M. JR. Jet Effects in Base and Afterbody Pressures of a Cylindrical Afterbody at Transonic Speeds, NACA RM L56 C21, 1958.
9. GLOSS, B. B. and SEWALL, W. G. Support–Sting Interference on Boat–tail Pressure Drag for Reynolds Numbers up to 70×10^6, AIAA Paper 83-0387, 1983.
10. VISWANATH, P. R. and RAJENDRA, G. Sting–Support Interference on Afterbody Drag at Transonic Speeds, NAL TM EA 8902, 1989.
11. SWAMY, M. S., AHMED, S. and SREENATH, G. S. Model Support System Interference on Zero-lift Drag at Transonic Speeds, AIAA paper 78-809, 1978.
12. KURN, A. G. Drag Measurements on a Series of Afterbodies at Transonic Speeds Showing the Effect of Sting Interference, RAE TR 66298, 1966.

APPENDIX 1: EXPRESSIONS FOR ESTIMATING STING CORRECTIONS

From Section 3.3, we have

$$\Delta C_{pb} = \Delta C_{pb(d_s)} + \Delta C_{pb(\theta)}$$

$$\Delta C_{D\beta} = \Delta C_{D\beta(d_s)} + \Delta C_{D\beta(\theta)}$$

The following expressions may be used for estimating sting corrections from the correlations.

(i) $\Delta C_{pb(d_s)} = 0{\cdot}08\,(d_s/d_b)^2$ . . . (A1)

for $0{\cdot}2 \leqslant d_s/d_b \leqslant 0{\cdot}75$

(For $d_s/d_b \geqslant 0{\cdot}75$, the mean line shown in Fig. 11 is to be used.)

(ii) $\Delta C_{pb(\theta)} = K_1\,(\theta^\circ)$ . . . (A2)

where $K_1 = 0{\cdot}015$ ($\beta = 4^\circ - 8^\circ$)
$= 0{\cdot}01$ ($\beta = 12^\circ - 16^\circ$)

(iii) $\Delta C_{D\beta(d_s)} = K_2\,(d_s/d_m)^{1{\cdot}35}$ . . . (A3)

where $K_2 = -0{\cdot}025$ ($\beta = 4^\circ$)
$= -0{\cdot}048$ ($\beta = 8^\circ$)
$= -0{\cdot}064$ ($\beta = 12^\circ$)
$= -0{\cdot}092$ ($\beta = 16^\circ$)

(iv) $\Delta C_{D\beta(\theta)} = K_3(\theta^\circ)$ . . . (A4)

where $K_3 = -0{\cdot}0025$ ($\beta = 4^\circ - 8^\circ$)
$= -0{\cdot}0045$ ($\beta = 12^\circ - 16^\circ$)

Note: Values of K_1, K_2 and K_3 may be linearly interpolated for intermediate values of β.